

The roles of the Ge-Te core network and the Sb-Te pseudo network during rapid nucleation-dominated crystallization of amorphous $\text{Ge}_2\text{Sb}_2\text{Te}_5$ revealed by anomalous x-ray scattering technique

S. Kohara^{1,*}, K. Ohara¹, L. Temleitner^{1,2}, K. Sugimoto¹, T. Matsunaga³, L. Pusztai², M. Itou¹, H. Ohsumi⁴, R. Kojima³, N. Yamada³, T. Usuki⁵, A. Fujiwara¹, and M. Takata^{1,4,6}

¹JASRI/ SPring-8, 1-1-1 Kouto, Sayo-cho, Sayo-gun, Hyogo 679-5198, Japan

²Wigner Research Centre for Physics, Hungarian Academy of Sciences, H-1525 Budapest, P. O. Box 49, Hungary

³Panasonic Corporation, 3-1-1 Yagumo-Nakamachi, Moriguchi, Osaka 570-8501, Japan

⁴RIKEN, 1-1-1 Kouto, Sayo-cho, Sayo-gun, Hyogo 679-5148, Japan

⁵Department of Material and Biological Chemistry, Faculty of Science, Yamagata University, 1-4-12 Koshirakawa, Yamagata 990-8560, Japan

⁶Department of Advanced Materials Science, School of Frontier Science, The University of Tokyo, 5-1-5, Kashiwanoha, Chiba 277-8561, Japan

*E-mail address: kohara@spring8.or.jp

ABSTRACT

We revealed for the first time, by modelling the amorphous structure of $\text{Ge}_2\text{Sb}_2\text{Te}_5$ based on synchrotron radiation anomalous X-ray scattering data, that germanium and tellurium atoms form a “core” Ge-Te network with ring formation. It is also suggested that the Ge-Te network can stabilize the amorphous phase at room temperature and can persist in the crystalline phase. On the other hand, antimony does not contribute to ring formation but constitutes a “pseudo” network with tellurium, in which the characteristic Sb–Te distance is somewhat longer than the covalent Sb–Te bond distance. This suggests that the Sb-Te pseudo network may act as a precursor to forming critical nuclei during the crystallization process. The findings conclude that the Ge-Te core network is responsible for the outstanding stability and rapid phase change of the amorphous phase while the Sb-Te pseudo network is responsible for triggering critical nucleation.

Key words: Structure, $\text{Ge}_2\text{Sb}_2\text{Te}_5$, anomalous x-ray scattering, Reverse Monte Carlo simulation

1. INTRODUCTION

Chalcogenide phase-change (PC) materials have been used in rewritable storage media, digital versatile disc – random access memory (DVD-RAM), DVD re-writable (DVD-RW), Blu-ray disc–rewritable (BD-RE) and non-volatile memory such as phase-change random access memory (PC-RAM). Numerous studies on the structure of amorphous (a-) $\text{Ge}_2\text{Sb}_2\text{Te}_5$ (GST)¹⁾ have been reported early in the last decade using experimental methods such as extended X-ray absorption fine-structure spectroscopy (EXAFS), high-energy X-ray diffraction (HEXRD) with the aid of reverse Monte Carlo (RMC) simulation, hard X-ray photoemission spectroscopy (HXPS) and theoretical methods. Thus the structure of amorphous (a)-GST and its relationship with rapid phase change is gradually being uncovered; the most recent results are reviewed in ref. 2. For understanding the role of each atom type beyond the nearest coordination distance, with a special focus on the question of why amorphous GST is stable at room temperature for a long time despite the fact that it can rapidly transform to the crystalline phase, we performed anomalous X-ray scattering (AXS) measurements at the Sb and Te K edges. It can provide information about the local environment of Sb and Te atoms beyond the nearest neighbour distance, in contrast to EXAFS. Furthermore, RMC modelling has been applied to AXS and HEXRD datasets on a-GST, while only to the latter for crystal (c-) GST, with a special focus on the connectivity of Ge-Te units and Sb-Te units beyond the nearest coordination distance.

2. EXPERIMENTS

The amorphous powder specimen for AXS measurements was prepared by laminating a 5-nm-thick ZnS-SiO₂ film on a glass disc (diameter 120 mm) and sputtering GST on it, to form a recording film of thickness 200–500 nm. The specimen was removed from the glass substrate using a spatula. The powdered sample was encapsulated in a thin-walled (10 μ m) silica glass tube (diameter: 0.5 mm; supplier: GLAS Müller, 13503 Berlin, Germany). The crystalline phase of GST was obtained by heating the amorphous powder in a tube at 413 K for 30 min.

The high-energy X-ray diffraction experiment on c-GST was carried out at room temperature at the SPring-8 high-energy XRD beamline BL04B2³⁾ using a two-axis diffractometer. The incident X-ray energy was 61.6 keV obtained from a Si 220 crystal monochromator. Diffraction patterns of the sample and an empty tube were measured in transmission geometry. The intensity of incident X-rays was monitored by an ionization chamber filled with Ar gas, and the scattered X-rays were detected by a Ge detector. A vacuum chamber was used to suppress air scattering around the sample. Collected datasets were corrected for absorption, background, and polarization. Details of data correction and normalization procedures are given in ref. 3.

Room temperature anomalous X-ray scattering measurements on a-GST were carried out at the SPring-8 single crystal structure analysis beamline BL02B1 using a 4-circle diffractometer. The monochromator of BL02B1 is a standard double-crystal Si (311) monochromator with a sagittal focusing system. Vertical focusing was achieved by a Pt coated total reflection mirror. AXS measurements were performed at 4 energies, 30.172 keV (Sb far edge), 30.422 keV (Sb near edge), 31.500 keV (Te far edge), and 31.750 keV (Te near edge). The intensity of incident X-rays was monitored by an ionization chamber filled with Ar gas, and the scattered X-rays were detected by a Ge detector. 6×10^5 counts were recorded at $Q=2 \text{ \AA}^{-1}$. Measured datasets were corrected for absorption, background, and fluorescence (K_β). The contribution of Compton scattering was subtracted and the fully corrected data were normalized to obtain total structure factor $S(Q)$. Differential structure factors $\Delta S(Q)$ for the Sb and Te edges were also calculated.

RMC simulation on a-GST was carried out by starting from an atomic configuration reported by Akola et al., that had been obtained by RMC/DF-MD simulation (Number of atoms: 460).⁴⁾ The experimental $\Delta S_{\text{Sb}}(Q)$ and $\Delta S_{\text{Te}}(Q)$ obtained from AXS measurement and $S(Q)$ obtained from high-energy X-ray diffraction measurement⁵⁾ were fitted simultaneously by employing the RMC++ code.⁶⁾ Modelling of c-GST was carried out using 7200 particles ($10 \times 10 \times 10$ unit cells) by the RMCPOW simulation procedure.⁷⁾ This method makes it possible to fit both Bragg- and diffuse scattering parts of the total pattern. The former is responsible for the periodic long range order of the average structure, while the latter is for the deviations from the average structure.

3. RESULTS & DISCUSSION

Figure 1(a) shows total scattering structure factors, $S(Q)$, for c-GST and a-GST. The diffraction pattern of c-GST exhibits sharp Bragg peaks and a diffuse scattering pattern, while only the latter appears for a-GST. It is demonstrated that $S(Q)$ of the RMC model (solid line) agrees well with experimental data (open circles). Differential structure factors, $\Delta S(Q)$, for Sb and Te obtained from AXS measurements are shown in Fig. 1(b). The differential structure factor of Sb, $\Delta S_{\text{Sb}}(Q)$ exhibits a peak at $Q=1 \text{ \AA}^{-1}$. This peak is also observed in HEXRD data for both phases (due to diffuse scattering present in c-GST), as shown in Fig. 1(a), and is more significant here than that in a-GeTe (GT).⁵⁾

To obtain information on partial correlations in real space, the partial pair distribution functions, $g_{ij}(r)$, for c-GST and a-GST, as derived from the RMC models, are compared in Fig. 2. As discussed in ref. 5, we can hardly see any structural similarity in experimental real-space functions beyond 3.5 \AA between c-GST and a-GST. Such differences between c-GST and a-GST are obvious in real space: c-GST exhibits significant oscillations indicating the long-range periodicity of the crystalline phase. Both the first Ge-Te and Sb-Te correlation lengths in a-GST are shorter than those in c-GST, due to the formation of covalent bonds in the former. The shortening of the nearest coordination distance is unambiguous for Ge-Te pairs, suggesting the formation of a Ge-Te covalent network accompanied by the reduction of

the coordination number in a-GST. On the other hand, the first Sb-Te correlation peak is observed at 2.9 Å whose position is not far away from that in c-GST.

Coordination numbers in a-GST are calculated up to 3.2 Å. In c-GST, both Ge and Sb are sixfold coordinated while the total coordination number of Te is 4.8 due to a vacancy on the Ge/Sb mixing site. These results are in line with the average structure of rocksalt, suggesting that disorder in the crystalline phase does not have any influence on average coordination numbers. Baker et al. reported on the basis of EXAFS measurements⁸⁾ that both Ge and Sb obey the so-called ‘8-N rule’ and that Te is overcoordinated in a-GST. On the other hand, Jóvári et al. reported a RMC model in which Ge, Sb, and Te all obey the ‘8-N rule’,⁹⁾ based on simultaneous RMC simulation of neutron, HEXRD and EXAFS datasets. Akola et al. reported overcoordinated Sb and Te on the basis of atomic configurations obtained by RMC/DF-MD simulation using HEXRD data only.⁴⁾ In our new RMC model, refined by employing AXS data, total coordination numbers for Ge, Sb, and Te are 3.83, 3.06, and 2.45, respectively. Antimony has a lower coordination number than in the previous RMC/DF-MD model ($N_{\text{Sb}}=3.31$ in ref. 4). As a result, now both Ge and Sb obey the ‘8-N rule’ and only Te is overcoordinated. These results agree well with results of EXAFS measurements⁸⁾ and are in line with discussions in ref. 2 and with that in Olson et al.’s argument, in which they mentioned the possibility of overcoordinated Te if there are no homopolar (Ge-Ge, Sb-Sb, Te-Te) bonds in a-GST.¹⁰⁾

As the simplest tool for analyzing correlations beyond the two-particle level, bond angle distributions of Te-Ge-Te and Te-Sb-Te triplets for c-GST and a-GST were calculated. c-GST exhibits peaks at 90° and 180° due to its rock salt structure. Bond angle distributions in a-GST show a similar trend, but peak widths increase and the magnitude of the peak at 180° significantly decreases. It is worth mentioning that the magnitude of the peak at 90° for a-GST is comparable to that for c-GST, although the bond angle becomes somewhat larger in a-GST, particularly for Te-Ge-Te triplets, due to small contributions

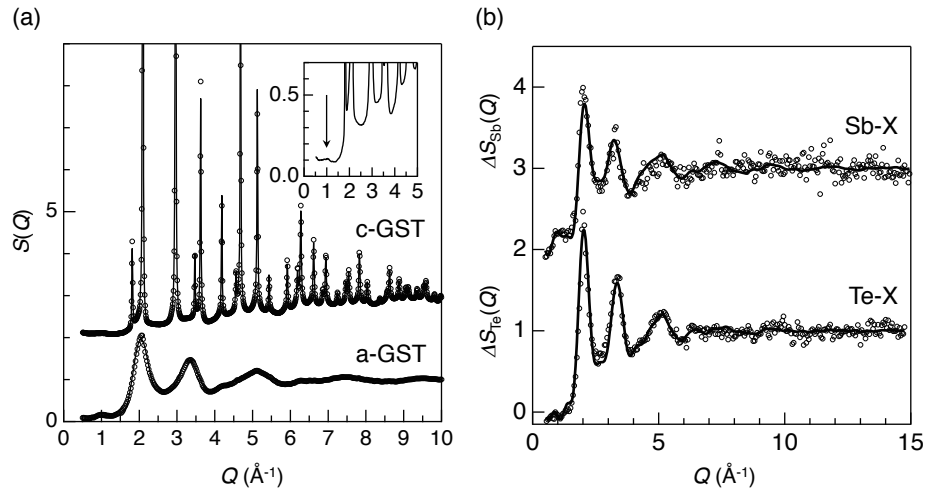


Fig. 1 Comparison between the experimental structure factors (open circle) and results of RMC modelling (solid line). (a) Total scattering data for c-GST and a-GST obtained by HEXRD measurements. The low Q part of c-GST data is enlarged in the inset. (b) $\Delta S(Q)$ for a-GST obtained by AXS measurements at Sb and Te K absorption edges.

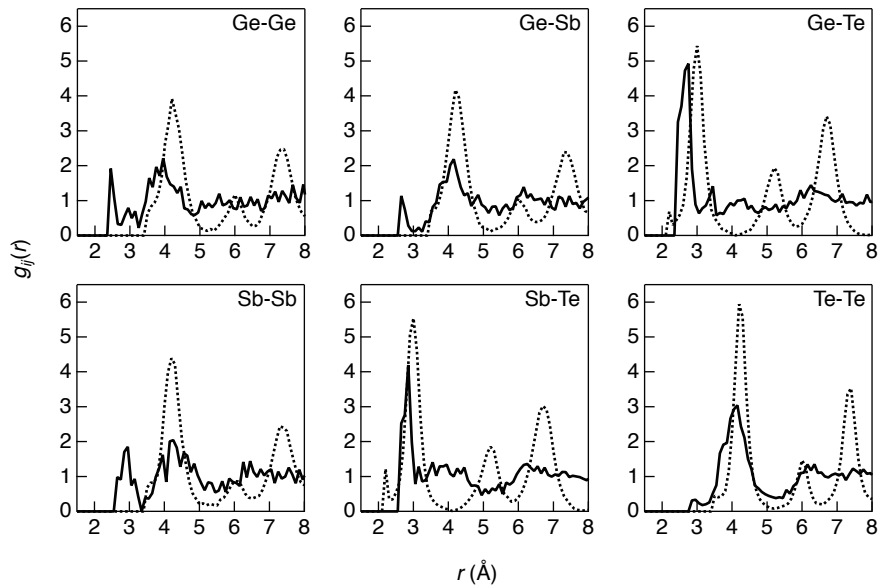


Fig. 2 Partial pair correlation functions, $g_{ij}(r)$, for c-GST (dotted line) and a-GST (solid line) obtained from the RMC models.

from tetrahedral Ge. This feature is consistent with the results of *ab initio* MD simulation reported by Caravati et al.¹¹⁾ Kim et al. mentioned the formation of threefold *p*-like bonding in a-GST¹²⁾ on the basis of HXPS data, which is consistent with the peaks at 90° and 180° in the bond angle distributions of our new RMC model.

For obtaining statistical structural features beyond the nearest coordination distance, ring statistics were calculated using a shortest path analysis.¹³⁾ As can be seen in Fig. 3(a), fourfold and sixfold rings consisting of ‘–Ge(Sb)–Te–’ units are dominant in c-GST. The existence of sixfold rings is due to the 20% vacancies on Ge/Sb mixing sites. As discussed in ref. 4, small ‘–Ge(Sb)–Te–’ rings such as fourfold, fivefold, and sixfold rings are dominant in a-GST. The numbers of rings consisting of ‘–Ge–Te–’ units and of ‘–Sb–Te–’ units in a-GST are shown in Fig. 3(b). Although the distribution of ‘–Ge(Sb)–Te–’ units has already been discussed in earlier studies,²⁾ we found for the first time that Ge–Te bonds form large numbers of fourfold and sixfold rings, while the contribution of Sb–Te bonds to the ring distribution is very small. Surprisingly our new RMC model obtained by the introduction of AXS data suggests that large fractions of fourfold and sixfold rings are mainly formed by Ge–Te bonds. Therefore it is suggested that the core network constructed by Ge–Te covalent bonds in a-GST is similar to that in c-GST, and that this core network plays an important role in stabilizing the amorphous phase at room temperature for long time.

To understand the atomic ordering by Ge–Te and Sb–Te bonds in detail, connectivities of atoms were calculated, with varying the maximum distance within which atomic pairs were considered to be connected. As can be seen in Fig. 4(a), about 60% of Ge–Te bonds up to 3.2 Å form a core

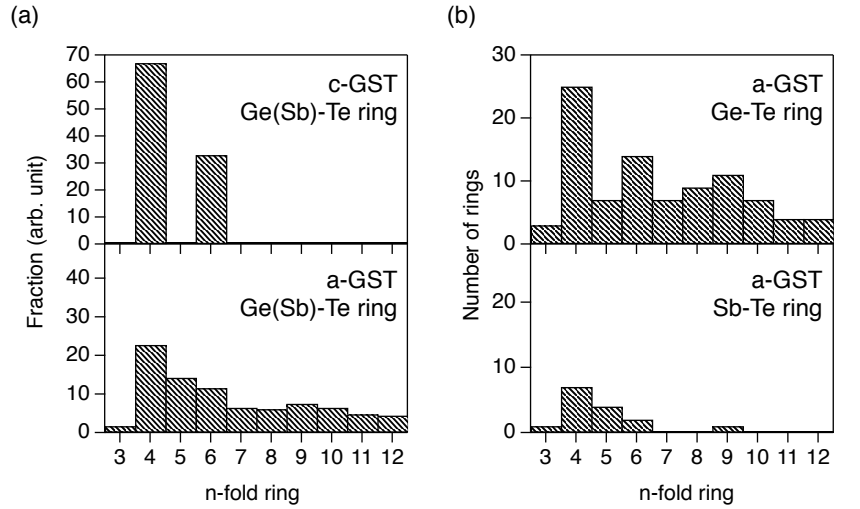


Fig. 3 Ring statistics for c-GST and a-GST obtained by the RMC models. (a) Normalized fraction of ‘–Ge(Sb)–Te–’ rings. (b) Numbers of ‘–Ge–Te–’ rings and ‘–Sb–Te–’ rings in a-GST. Total number of ‘–Ge(Sb)–Te–’ rings are normalized since number of particles in the simulation box are not same in c-GST and a-GST. The numbers of ‘–Ge–Te–’ rings and ‘–Sb–Te–’ rings clearly show that ‘–Ge–Te–’ rings form covalent network and ‘–Sb–Te–’ rings do not contributed to network in a-GST.

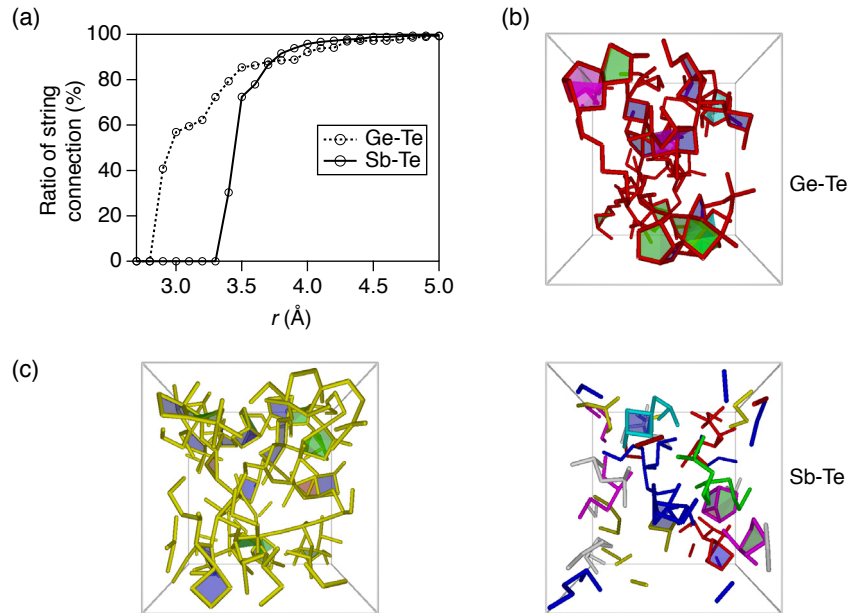


Fig. 4 Atomic configuration and connectivity of Ge–Te and Sb–Te in a-GST obtained by the RMC model. (a) Connectivity of Ge–Te and Sb–Te with different r_{\max} . (b) Atomic configuration of Ge–Te and Sb–Te (connectivity of Ge–Te and Sb–Te considered up to 3.2 Å). (c) Atomic configuration of Sb–Te (connectivity of Sb–Te considered up to 3.5 Å). The threefold, fourfold, fivefold, and sixfold rings are highlighted by red, blue, green, and light blue, respectively.

network whereas Sb-Te bonds up to 3.2 Å do not form such a network. This distance corresponds to the covalent bond distance determined by DF-MD simulation⁴⁾ and both Ge and Sb satisfy the ‘8-N rule’ at 3.2 Å in our new RMC model ($N_{\text{Ge}}=3.83$ and $N_{\text{Sb}}=3.06$). Atomic configurations of Ge-Te and Sb-Te with bonds considered up to 3.2 Å are shown in Fig. 4(b). It can be clearly distinguished that Ge-Te bonds form a core network, which stabilizes the amorphous phase, whereas Sb-Te bonds do not. Furthermore it is evident that Ge-Te bonds form large fractions of fourfold (highlighted by blue) and sixfold (highlighted by light blue) rings, which can be recognized as crystalline nuclei as shown in Fig. 2d of ref. 14. On the other hand, about 70 % Sb-Te correlations form a pseudo network, as can be seen in Figs. 4(a) and 4(c), when bonds are considered up to 3.5 Å (this way, the coordination numbers of Te around Ge ($N_{\text{Ge-Te}}$) and Sb ($N_{\text{Sb-Te}}$) are 4.08 and 3.08, respectively). In other words, the pseudo Sb-Te network becomes visible when we extend the correlation distance up to 3.5 Å, while such a feature cannot be observed for Ge-Te connectivities.

On the basis of structural features in a-GST found above, we illustrate the phase-change scheme in Fig. 5. As highlighted by red in Fig. 5(a), Ge-Te bonds significantly contribute to the network manifested by fourfold rings. Therefore Ge and Te can be recognized as network forming elements that stabilize the amorphous phase at room temperature for long time. The core Ge-Te network may remain in the crystalline phase, which feature explains rapid crystallization. As highlighted by yellow in Fig. 5(b), the Sb-Te correlations beyond the nearest coordination distance form a pseudo Sb-Te network. This unusual atomic ordering in terms of Sb-Te correlations can be ascribed to the combination of two positively charges atoms (Ge, -0.22 electrons; Sb, 0.32 electrons; Te, 0.22 electrons¹⁵⁾) and allows the amorphous phase to form critical nuclei via forming Sb-Te bonds by small atomic displacements of antimony and tellurium atoms. Thus our finding can reasonably explain the reason why the crystallization of amorphous GeTe (a-GT) is very fast in PC-RAM¹⁶⁾ and the reason why the crystallization of a-GST is faster than a-GT in DVD.¹⁷⁾

4. CONCLUSION

We found that germanium forms a covalent core network with tellurium to stabilize the amorphous phase at room temperature, which core network can remain in the crystalline phase. Antimony maintains an atomic ordering with tellurium beyond the Sb-Te covalent bond distance in a-GST; these atomic pairs can rapidly fit into the Ge-Te core network in the crystalline phase at higher temperature induced by a laser irradiation. This behavior is similar to the Sb local environment of distorted 3 + 3 octahedron¹⁴⁾ found in another phase change material, $\text{Ag}_{3.5}\text{In}_{3.8}\text{Sb}_{75.0}\text{Te}_{17.7}$ (AIST), in which Sb possesses locally extra 3 neighbours beyond the nearest coordination covalent bond distance. Our finding can reasonably explain the roles of germanium and antimony in DVD with respect to rapid phase change and durability. Thus it is demonstrated that the observation of network formation is important to reveal the origin of rapid phase change at atomic level. This finding is a crucial new key concept for designing new PC materials with excellent durability.

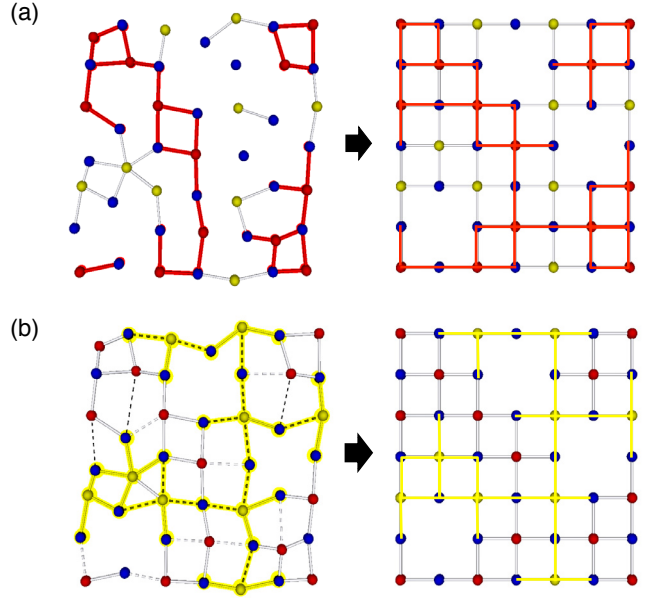


Fig. 5 Schematic drawing for phase-change process in a-GST. (a) highlights Ge-Te core network. (b) highlights Sb-Te pseudo network. Red, Ge; yellow, Sb; blue, Te. Red colored sticks show Ge-Te bonds up to 3.2 Å. Yellow colored sticks show Sb-Te bonds up to 3.2 Å and yellow colored dotted lines show Sb-Te correlations between 3.2 to 3.5 Å.

REFERENCES

1. M. Wuttig and N. Yamada, *Nature Mater.* **6** (2007) 824
2. D. Lencer, M. Salinga, and M. Wuttig, *Adv. Mater.* **23** (2011) 2030
3. S. Kohara, M. Itou, K. Suzuya, Y. Inamura, Y. Sakurai, Y. Ohishi, and M. Takata, *J. Phys.: Condens. Matter* **19** (2007) 506101
4. J. Akola, R. O. Jones, S. Kohara, S. Kimura, K. Kobayashi, M. Takata, T. Matsunaga, R. Kojima, and N. Yamada, *Phys. Rev. B* **80** (2009) 020201
5. S. Kohara, K. Kato, S. Kimura, H. Tanaka, T. Usuki, K. Suzuya, Y. Moritomo, T. Matsunaga, N. Yamada, Y. Tanaka, H. Suematsu, and M. Takata, *Appl. Phys. Lett.* **89** (2006) 201910
6. O. Gereben, P. Jónvári, L. Temleitner, and L. Pusztai, *J. Optoelectron. Adv. Mater.* **9** (2007) 3021
7. A. Mellergård and R. L. McGreevy, *Acta. Cryst.* **55** (1999) 783
8. D. A. Baker, M. A. Paesler, G. Lucovsky, S. C. Agarwal, and P. C. Taylor, *Phys. Rev. Lett.* **96** (2006) 255501
9. P. Jónvári, I. Kaban, J. Steiner, B. Beuneu, A. Schöps, and M. A. Webb, *Phys. Rev. B* **77** (2008) 035202
10. J. K. Olson, H. Li, and P. C. Taylor, *J. Ovonic Res.* **1** (2005) 1
11. S. Caravati, M. Bernasconi, T. D. Kühne, M. Krack, and M. Parrinello, *Appl. Phys. Lett.* **91** (2007) 171906
12. J. J. Kim, K. Kobayashi, E. Ikenaga, M. Kobata, S. Ueda, T. Matsunaga, K. Kifune, R. Kojima, and N. Yamada, *Phys. Rev. B* **76** (2007) 115124
13. L. Guttman, *J. Non-Cryst. Solids* **116** (1990) 145
14. T. Matsunaga, J. Akola, S. Kohara, T. Honma, K. Kobayashi, E. Ikenaga, R. O. Jones, N. Yamada, M. Takata, and R. Kojima, *Nature Mater.* **10** (2011) 129
15. J. Akola and R. O. Jones, *J. Phys.: Condens. Matter* **20** (2008) 465103
16. G. Bruns, P. Merkelbach, C. Schlockermann, M. Salinga, M. Wuttig, T. D. Happ, J. B. Philipp, and M. Kund, *Appl. Phys. Lett.* **95** (2009) 043108
17. J. H. Coombs, A. P. J. M. Jongenelis, W. v. Es-Spiekman, and B. A. J. Jacobs, *J. Appl. Phys.* **78** (1995) 4918